Distributed Control for a Microgrid Cluster: Implementation and Experimental Validation

Carrasco González, David; Sarrias Mena, Raúl; Horrillo Quintero, Pablo; Hosseini, Ehsan; Llorens Iborra, Francisco; Fernández Ramírez, Luis Miguel

Published in:
2024 IEEE International Conference on Environment and Electrical Engineering and 2024 IEEE Industrial and Commercial Power Systems Europe, EEEIC / I and CPS Europe 2024, 2024

DOI (link to publication from Publisher):
10.1109/EEEIC/ICPSEurope61470.2024.10751158

Publication date:
2024

Document Version:
Camera ready

Citation for published version (IEEE):
D. Carrasco-González, R. Sarrias-Mena, P. Horrillo-Quintero, E. Hosseini, F. Llorens Iborra, and L. M. Fernández-Ramirez, "Distributed Control for a Microgrid Cluster: Implementation and Experimental Validation" Proceedings - 2024 IEEE International Conference on Environment and Electrical Engineering and 2024 IEEE Industrial and Commercial Power Systems Europe, EEEIC / I and CPS Europe 2024, 2024, doi: 10.1109/EEEIC/ICPSEurope61470.2024.10751158.

979-8-3503-5518-5/24/$31.00 ©2024 IEEE

Distributed Control for a Microgrid Cluster: Implementation and Experimental Validation

David Carrasco-González
SURET Research Group
Department of Electrical Engineering
University of Cadiz
Algeciras, Spain
david.carrasco@uca.es

Raúl Sarrias-Mena
SURET Research Group
Department of Engineering in Automation, Electronics and Computer Architecture and Networks
University of Cadiz
Algeciras, Spain
raul.sarrias@uca.es

Pablo Horrillo-Quintero
SURET Research Group
Department of Electrical Engineering
University of Cadiz
Algeciras, Spain
pablo.horrillo@uca.es

Ehsan Hosseini
SURET Research Group
Department of Electrical Engineering
University of Cadiz
Algeciras, Spain
ehsan.hosseini@uca.es

Francisco Llorens-Iborra
SURET Research Group
Department of Electrical Engineering
University of Cadiz
Algeciras, Spain
francisco.llorens@uca.es

Luis M. Fernández-Ramírez
SURET Research Group
Department of Electrical Engineering
University of Cadiz
Algeciras, Spain
luis.fernandez@uca.es

***Abstract*—In response to growing energy demands and concerns about climate change, microgrid clusters (MGCs) are gaining widespread attention. Their ability to integrate technologies for energy consumption, generation, and storage in AC, DC or a compound of both offer a high degree of flexibility and resiliency. This research introduces a new control strategy for an MGC composed of two MGs interconnected to a local grid via a point of common coupling. The first one is a DC MG comprising an ultracapacitor (UC), wind turbine (WT), DC loads and hydrogen system. The second is an AC MG with a battery bank, AC loads and photovoltaic (PV) generator. The control strategy employs local controllers for each device and distributed control via two control agents, coordinating the power distribution among the energy storage systems (ESSs) of the MGC. This system is tested and validated on a real-time experimental setup, using two Raspberry Pi microcontrollers and an OPAL-RT unit, under different working conditions. The results obtained in this work show that the control strategy implemented in the MGC works correctly.**

Keywords—Control agent, distributed control, microgrid cluster, real-time simulation

I. Introduction

In the contemporary world, the fight against climate change and international agreements to exclude fossil fuels have propelled renewable energy sources to the vanguard of electricity generation, removing environmentally damaging emissions with low carbon alternatives [1]. Furthermore, there is a high pressure from rising power demand in factories and cities. Thus, these facts are pushing the development of independent and smaller grids, called as microgrids (MGs) [2]. These solutions include increased energy efficiency, minimized carbon emissions, improved power reliability and quality, and cost-effective operation [3].

MGs revolutionize energy independence by integrating diverse renewable sources, storage solutions and local loads within specified limits, creating a controllable and autonomous system [4]. Researchers initially investigated the AC MGs, due to their compatibility with existing infrastructure. But in the modern-day, DC MGs are being developed [5]. In this sense, MGs can offer enhanced flexibility and adaptability by supporting DC, AC, or hybrid operation, allowing them to integrate seamlessly with diverse grid configurations and requirements [6].

Regarding to their relationships with the environment, they can be stand-alone, which is the typical situation for remote locations [7], or integrated with a local grid via a point of common coupling (PCC). This latter situation can produce a grid-connected and an islanded state. In the first state, the power mismatches in the MG are solved by the local grid [8]. In the second state, the electricity generated in the MG must be used by the loads or channelled into energy storage systems (ESSs) for future usage [9].

Coordinating and interconnecting multiple nearby microgrids creates a microgrid cluster (MGC), offering numerous advantages such as simplifying component integration, decentralising the power grids, enhancing sustainability, reliability, efficiency and resilience and promoting local electricity production and consumption [10].

In the context of MGC control, there are different types of architectures in order to achieve their specific objectives [11]. One of them is the distributed architecture, which uses control agents to reach objectives by coordinating the operation of individual MGs. In this regard, control agents provide references signals to individual energy sources and these references can be determined through diverse manners [12], [13].

This work presents the testing and validation of a new control strategy for a MGC. The MGC, consisting of an AC MG and DC MG interconnected to a local grid, is implemented in an experimental configuration using Raspberry Pi and OPAL-RT units. The control strategy uses local control of the devices and distributed control achieved through two control agents.

The rest of the work is divided into a description of the configuration and control strategy of the system in Section II.

This work was partially supported by Ministerio de Ciencia e Innovación, Agencia Estatal de Investigación, FEDER, UE (Grant PID2021-123633OB-C32 supported by MCIN/AEI/10.13039/501100011033/ FEDER, UE).

Section III details the experimental configuration developed for the MGC. Section IV shows and discusses the experimental results. Ultimately, the conclusion of this work are presented in Section V.

II. Control and Configuration

This paper presents a hybrid grid-connected DC/AC MGC configuration that is shown in Fig 1. Each device of the MGC is controlled and operated individually, while two supervisor control agents are responsible to regulate the energy dispatch between MGs, one control agent per MG. It is noteworthy that the controlled components in each MG are the ESSs, while the RETs operate according to the maximum power point tracking (MPPT) strategy. The main goal of the control agents is to perform an efficient energy distribution between MGs to fulfil DC and AC loads, avoiding the consumption of the local grid. The following subsections detail the control and configuration systems of the MGC.

A. Local Grid

The AC local grid in the system is simulated as an ideal three-phase voltage source. This device has a consistent voltage and frequency, representing an infinite power grid.

The primary grid is linked to the PCC alongside the DC and AC MGs. Throughout this paper, the system consistently functions in grid-connected state, with no consideration given to islanded operation. As the local grid maintains the frequency and voltage at the PCC, no control measures are necessary, and the reactive and active power exchanged with the local grid are autonomously adjusted to maintain power equilibrium and prevent frequency and voltage variations.

B. DC MG

The DC MG designed in this work comprises a wind turbine (WT) and several ESSs connected to a 1100 V DC bus. The ESSs consist of a hydrogen system formed by a fuel cell (FC) and an electrolyzer (EZ), and an ultracapacitor (UC). Furthermore, DC loads are connected to this MG.

The WT is represented as a synchronous generator in a sixth-degree system. Subsequently, the WT is linked to the DC bus through an unregulated bridge rectifier, which converts the AC energy produced by the WT into DC energy, and a DC step-up converter, which adjusts the speed of the wind turbine to attain optimal operation in response to fluctuating wind speeds.

Concerning the ESSs architecture, a half-bridge converter is employed to link the UC to the DC bus. This configuration permits both discharging and charging of the UC, facilitating the flow of energy bidirectionally. As only power supply to this MG is possible for the FC, a step-up converter is utilized for this component. Likewise, a buck converter is applied to the EZ, as it can solely consume power from the shared DC bus. The EZ is simulated using a combination of DC voltage source and a serial resistance, the FC is simulated implementing a regulated DC voltage source with an incorporated diode, and the UC is simulated using an ideal condenser with a serial resistance.

The DC bus directly supplies to the DC loads. Only a disconnector is used to disconnect and connect the DC loads.

This MG is linked to the PCC with the AC MG and the local grid through a voltage source converter (VSI). This converter ensures stable DC bus voltage by compensating for active power variations due to the load changes and wind speed [14]. Additionally, it converts DC power into AC power for the grid.

C. AC MG

The AC MG is composed of a battery energy storage system (BESS), PV generators and AC loads. A power transformer of 480/600 V is considered to connect the PV generators and the BESS to the main grid.

The PV power plant selected is based on the model described in [15] ,which consists of a real controlled current source connected with a parallel diode. To perform the MPPT strategy, the PV power plant is controlled through a Perturbe&Observe (P&O) algorithm. The duty cycle of a step-up converter is responsible to control the PV power plant DC output voltage. Furthermore, a VSI is used to convert the DC into AC. Because of the PV generators are connected to a local grid, the frequency is forced by the local grid. The control of the VSI is performed into the direct-quadratic (*dq*) frame, employing a cascaded control loop based on PI controllers [14].

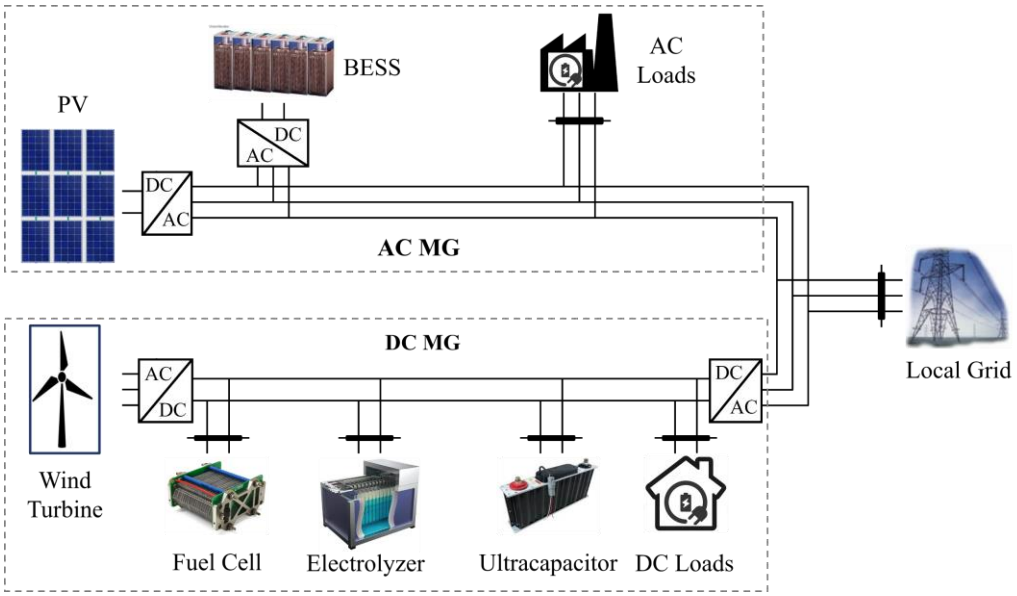

Fig. 1. Configuration of the system.

A Lithium-Ion BESS is utilized within this MG as controlled component to smooth out the fluctuations of the PV power plant. The BESS is simulated implementing a real controlled voltage source. A VSI is responsible to connect the BESS to the AC bus. The VSI is managed to control the reactive and active power exchange.

Moreover, the AC MG is complemented by AC loads. Several three-phase local loads, modelled as resistance-inductance (RL) are introduced. These loads are disconnected and connected in a non-seasonable manner to test the response of the control agents and MGs controllers under dynamically changing AC loads.

D. Local Controllers

In this subsection, the local controllers implemented for each device in the MGC are summarized. The PV power plant employs the MPPT algorithm to optimize its power generation according to the varying incident solar radiation. For the WT, its speed is regulated to track the optimal power curve under a variable wind speed.

The flow of power among the ESSs is regulated to follow the setpoints generated by each control agent, using PI controllers. Thus, the UC, FC, BESS and EZ controllers have to realize this task. Under these conditions, the BESS and the UC controllers can receive positive and negative active power reference values, allowing the charge and discharge of them. The EZ and FC controllers are limited to receiving single-sign signals. A negative value enables power consumption for the EZ, while a positive value enables power generation for the FC.

The local loads are connected/disconnected into their respective MGs employing time-controlled circuit breakers at different time intervals. Additionally, they do not need any particular control strategy, because the demand that they generate is taken into account in the control agents.

E. Control Agents

The control agents are required to monitor, manage the energy exchange among the ESSs and ensure the energy balance. In this regard, one control agent is proposed for the DC MG and one for the AC MG. Both control agents are based on the assumptions that the generation devices that make up an MG provides to a single generation pool of that MG, and the consumption devices that make up an MG contribute to a single consumption pool of that MG.

In first place, the main goal of each control agent is to satisfy the needs of its MG with their own ESSs and then to satisfy the power imbalances of the other MG. This encompasses covering power imbalances during maximum generation and minimum demand, as well as during maximum demand and minimum generation. Thus, when the generation power is not equal to the power demanded within the MG, the ESSs of that MG cover this power imbalance, according to their inherited characteristics.

In the AC MG, the BESS is used depending on its state-of-charge (SOC) to prevent it overcharge and undercharge conditions. In the other MG, the EZ consumes energy, the FC supplies energy and the UC compensates transient and fast power mismatches, generated by the limited dynamic response of the hydrogen system. Finally, minimum levels of power usage and production are guaranteed for the hydrogen system to avoid disconnections.

Then, in the DC MG control agent, the power imbalance between generation, demand and a possible AC MG power imbalance is first checked. If the power imbalance is positive, the EZ consumes the surplus energy while the FC is at the minimum power usage level. In the opposite case, the FC generates the missing power while the EZ is at the minimum power usage level. Subsequently, to calculate the active power setpoint for the UC, the combined output power of the EZ and FC is subtracted from the combined reference power of both devices. If the active power of these devices is perfectly regulated, the active output powers and their references only deviate momentarily, depending on the time constant of each device. Ultimately, if the contribution of the ESSs of this MG is not sufficient to satisfy the power mismatch, the other MG is responsible for covering this imbalance.

In the AC MG control agent, the power imbalance between the generation, demand and the possible DC MG power imbalance is first checked. If the power imbalance is positive, the BESS stores the surplus energy, and generates energy when the imbalance is negative. Secondly, the SOC of the BESS is measured to determine whether it can store or supply energy. The BESS cannot consume additional energy when its SOC is high, and conversely, cannot discharge further when its SOC is low. When it is in a medium state, it can be discharged or charged according to its SOC. Ultimately, if the BESS contribution is not enough to cover the power imbalance, the other MG is responsible for covering this imbalance.

While the ESSs of each MG play a critical role, the local grid acts as a safety net. It guarantees power balance at the PCC when the combined capacity of all ESSs is insufficient to address individual MG power imbalances.

III. Experimental Setup

This section details a comprehensive overview of the real-time experimental setup, designed to emulate and test the proposed MGC. Section III.A introduces the architecture of the configuration, while Section III.B examines the communication employed in the experimental setup.

A. Experimental Setup

As illustrated in Fig. 2, the experimental setup utilizes two Raspberry Pi-based microcontrollers and an OPAL-RT 4512 unit.

OPAL-RT, specifically the OPAL-RT 4512 unit, is a hardware-in-the-loop (HIL) emulation system that allows to emulate the MGC in real-time. It seamlessly integrates models created in MATLAB/Simulink into hardware in real-time. It uses the RT-LAB software to create, load, run and monitor the model, ensuring a high-performance simulation experience.

Raspberry Pi is a cost-effective and portable solution, programmable in Python, providing a platform for designing and implementing MG controls and management algorithms. In this work, Python 3.7 is the version selected for the programming language.

In this work, the local controllers and MCG are built in MATLAB/Simulink and transferred to the OPAL-RT 4512 real-time simulator via RT-LAB. For computational performance efficiency and real-time execution, the MGC is divided into three subsystems: the Master Subsystem, the Slave Subsystem, and the Scope Subsystem. The control agents are executed in two different Raspberry Pi

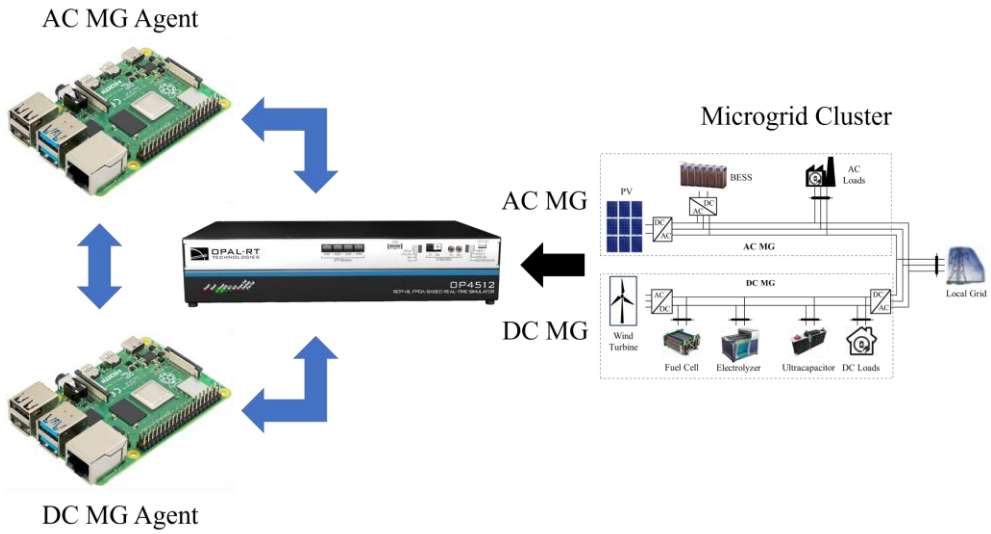

Fig. 2. Experimental configuration architecture.

microcontrollers, one for each MG. This experimental setup streamlines development and effectively represents the intricate interactions of the MGC.

B. Data Communication Protocol

For versatile data communication protocol in the real-time simulation, OPA-RT offers industry-standard communication protocols [16]. Among all the alternatives, TCP/UDP IO Interface is a user-friendliness and versatile choice that facilitates the data transmission through UDP and operates through a server-client communication model [17].

In this protocol, the OPAL-RT simulator and the Raspberry Pi microcontrollers use an ethernet network, where the real-time communication is established by sharing one IP address for each device and one UDP port for each communication link among the devices. Each device has two UDP ports as it communicates with the other two devices. This data communication protocol facilitates seamless data exchange. The IP address and the UDP ports must be introduced in each equipment for the correct communication.

The steps involved in sending information are as follows: each Raspberry Pi microcontroller receives the demanded and generated energy from its respective MG, the real-time information from the ESSs and the possible power imbalance of the other MG. In each Raspberry Pi microcontroller, the control agent obtains the setpoint power for the ESSs and the possible power imbalance of its respective MG. Finally, the Raspberry Pi microcontroller returns the data calculated.

The data exchange is limited in the data communication process by the decimation factor of the OPAL-RT unit, the sleep time of each Raspberry Pi microcontroller, and the time step of the simulation.

IV. Experimental Results

In this section, the MGC is emulated in the experimental setup to validate and verify the system performance and the control strategy developed for the MGC, under different working conditions in a real-time test with a duration of 10 s.

In the experimental test, the wind speed and the incident solar radiation are variable parameters, which generate fluctuations in the energy produced by the PV generators and WT. Additionally, the local loads are connected/disconnected into their respective MGs at diverse specified intervals, varying the power demanded by the MGs. The experiment begins with the BESS at a medium SOC of 50%.

A. DC MG

Fig. 3 illustrates the power generated (P_{WT}) and consumed ($P_{Load_{DC}}$) within the DC MG and the power imbalance of the AC MG (ΔP_{AC}). As evidenced, the WT power generation varies throughout the experimental test as a function of wind speed. With respect to the demanded energy, it varies depending on the connection/disconnection of the local loads from the DC bus. As mentioned, the loads are introduced as constant values, but it has small fluctuations in the power demanded owing to the slight voltage changes in this bus. This effect does not occur in the AC bus thanks to the local grid.

Finally, the evolution of the power imbalance of the AC MG indicates that there is an imbalance of that MG throughout the simulation. This imbalance may occur due to the fact that the BESS cannot fully balance power within its own MG or the medium SOC of the BESS.

Fig. 4 presents the flow of power between the ESSs of the DC MG and their references. All these devices successfully track their active power references, validating the performance of the local controllers. During periods of excess consumption (2.5 s - 3 s), the FC supplies the deficit within

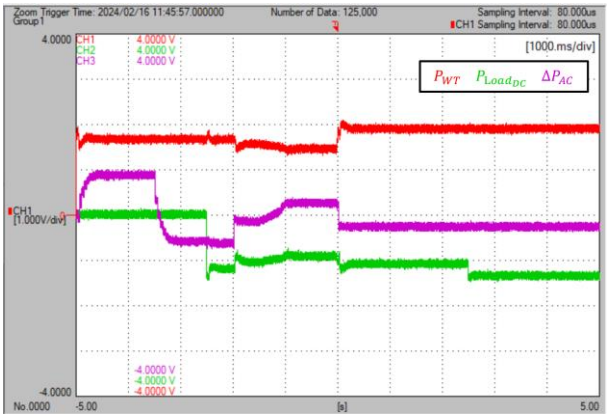

Fig. 3. Demanded and generated power within the DC MG and power imbalance of the AC MG.

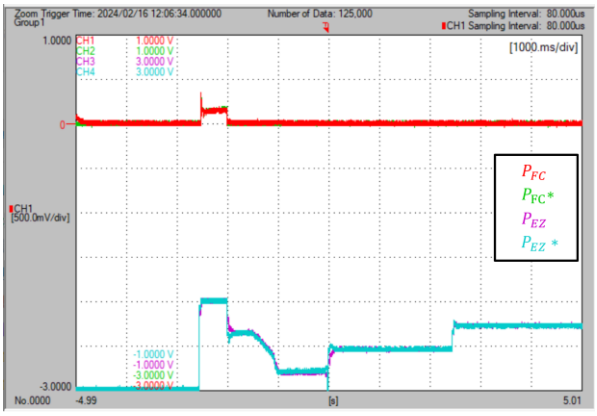

(a)

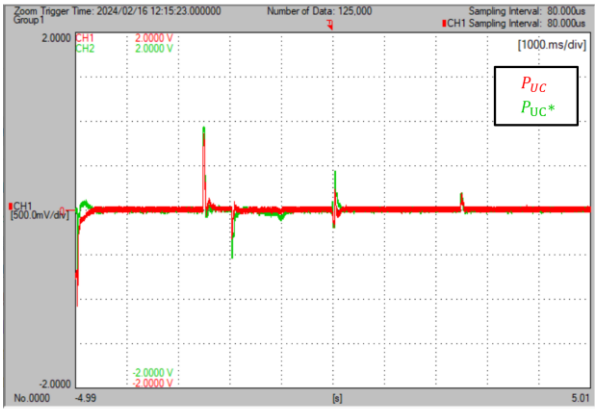

(b)

Fig. 4. Flow of active power of the ESS within the DC MG: (a) FC and EZ, and (b) UC.

the MG, while the EZ remains inactive at its minimum level. Conversely, during periods of surplus generation, the EZ absorbs the excess energy, and the FC remains inactive. It is important to note that from 0 seconds to 2.5 seconds, the EZ is at full capacity and cannot absorb any additional energy, causing that this MG cannot cover this surplus.

Lastly, the UC manages during transients with long power excursions that tend to zero when the MGC stabilizes.

The DC bus voltage is shown in Fig. 5. The experimental results demonstrate that the voltage is correctly adjusted around its setpoint value. As expected, the changes in this MG generate changes in this voltage, however, it is satisfactorily

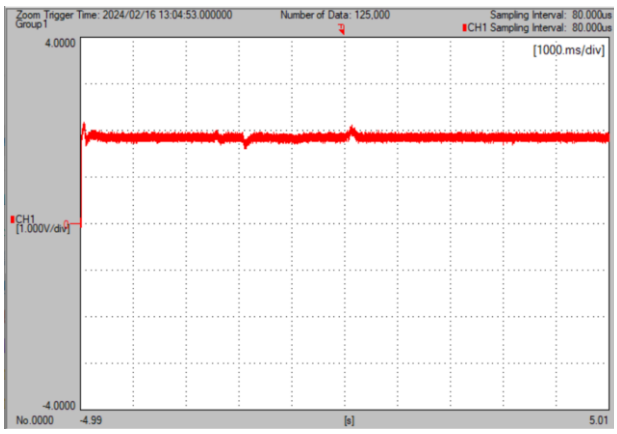

Fig. 5. DC bus voltage.

controlled by the cascaded control loop developed in the VSI of this MG.

B. AC MG

The power consumed ($P_{Load_{AC}}$) and generated (P_{PV}) within the AC MG and the power imbalance of the DC MG (ΔP_{DC}) is illustrated in Fig. 6. As evidenced, the power generated by the PV power plant varies throughout the experimental test as a function of the solar radiation. The consumed energy varies depending on the connection/disconnection from the AC bus at different specified intervals.

The evolution of the power imbalance of the DC MG indicates that there is an imbalance at the beginning of the simulation, which is resolved after 2.5 s. This imbalance is due to the fact that the EZ cannot balance the power within its own MG, as seen in Fig. 4.

The flow of power of the BESS and its reference are illustrated in Fig. 7. The BESS successfully tracks its reference, validating the local controllers. Furthermore, when generation exceeds demand within this MG, the BESS stores energy (approximately between 0 and 1.5 s, and between 3.75 and 5 s) and supplies energy in the remainder of the simulation. Since the BESS is at 50 % of its SOC, the BESS absorbs and supplies energy according to its SOC, confirming the power imbalance of this MG.

C. Local Grid

Fig. 8 illustrates the flow of active power with the local grid. The local grid participates when the ESSs of the two

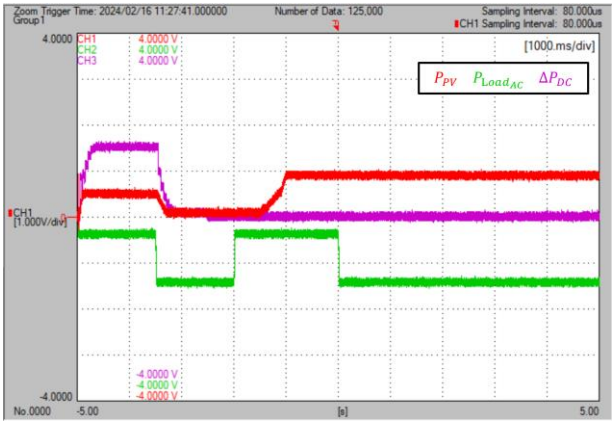

Fig. 6. Demanded and generated power within the AC MG and power imbalance of the DC MG.

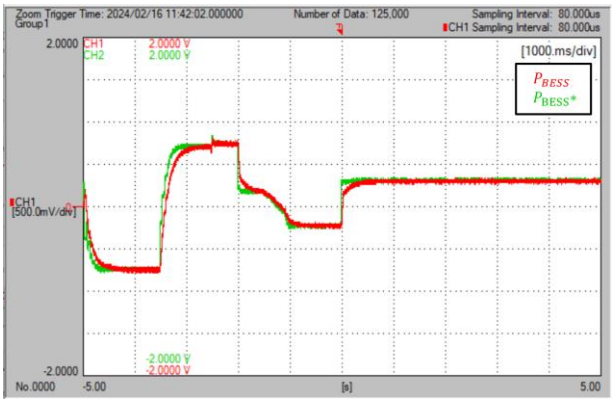

Fig. 7. Flow of active power of the BESS.

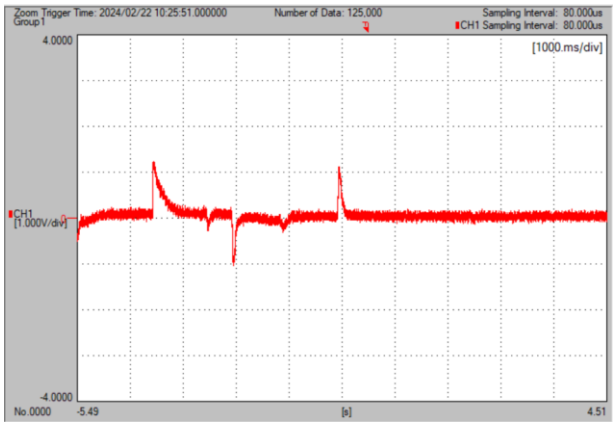

Fig. 8. Flow of active power with the local grid.

MGs cannot cover the power imbalances generated by the application of the different operating conditions. In most cases, the local grid supplies and absorbs the imbalance during the generated transients and, when the power is re-established in both MGs, the power exchange returns to tend to zero again.

Thus, this section provides compelling evidence, through its results, that the MGC, its local controllers, and both control agents operate adequately.

V. Conclusion

This work developed the validation and verification of a new control strategy for a MGC in a real-time experimental setup.

The MGC was constituted by a DC MG, composed of DC loads, WT, hydrogen system and UC, and an AC MG, composed of AC loads, a PV power plant and a BESS, interconnected to a local grid. The control strategy was composed of the local control of each device within the MGC, and a distributed control based on a control agent for each MG. The real-time experimental setup was based on the use of an OPAL-RT 4512 simulator emulating the MGC and two Raspberry Pi-based microcontrollers, each integrating the control agent for its respective MG.

The validation and verification of the system was executed in a real-time test under various working scenarios, such as variable incident solar radiation and wind speed, and the disconnection and connection of the local loads at different time intervals. The experimental results demonstrate successful performance of the MGC, local controllers, and both control agents. Additionally, the implemented control strategy in the MGC effectively minimized the local grid intervention.

References

[1] B. Bergougui, “Moving toward environmental mitigation in Algeria: Asymmetric impact of fossil fuel energy, renewable energy and technological innovation on CO2 emissions,” *Energy Strategy Reviews*, vol. 51, p. 101281, Jan. 2024, doi: 10.1016/J.ESR.2023.101281.

[2] M. H. Taheri, M. Seiiedhoseiny, M. Mohammadpourfard, and G. G. Akkurt, “Future Trends of Hybrid Energy Systems,” *Reference Module in Earth Systems and Environmental Sciences*, Jan. 2023, doi: 10.1016/B978-0-323-93940-9.00062-1.

[3] J. Zhou, Z. Weng, J. Li, and X. Song, “Reliability evaluation, planning, and economic analysis of microgrid with access to renewable energy and electric vehicles,” *Electric Power Systems Research*, vol. 230, p. 110252, May 2024, doi: 10.1016/J.EPSR.2024.110252.

[4] M. Uddin, H. Mo, D. Dong, S. Elsawah, J. Zhu, and J. M. Guerrero, “Microgrids: A review, outstanding issues and future trends,” *Energy Strategy Reviews*, vol. 49, p. 101127, Sep. 2023, doi: 10.1016/J.ESR.2023.101127.

[5] L. de Oliveira-Assis *et al.*, “Optimal energy management system using biogeography based optimization for grid-connected MVDC microgrid with photovoltaic, hydrogen system, electric vehicles and Z-source converters,” *Energy Convers Manag*, vol. 248, pp. 196–8904, 2021, doi: 10.1016/j.enconman.2021.114808.

[6] S. Patel, A. Ghosh, and P. K. Ray, “Adaptive power management in PV/Battery integrated hybrid microgrid system,” *PESGRE 2022 - IEEE International Conference on “Power Electronics, Smart Grid, and Renewable Energy,”* 2022, doi: 10.1109/PESGRE52268.2022.9715905.

[7] T. E. Sati, M. A. Azzouz, and M. F. Shaaban, “Adaptive harmonic-based protection coordination for inverter-dominated isolated microgrids considering N-1 contingency,” *International Journal of Electrical Power & Energy Systems*, vol. 156, p. 109750, Feb. 2024, doi: 10.1016/J.IJEPES.2023.109750.

[8] F. N. Budiman, M. A. M. Ramli, H. R. E. H. Bouchekara, and A. H. Milyani, “Optimal scheduling of a microgrid with power quality constraints based on demand side management under grid-connected and islanding operations,” *International Journal of Electrical Power & Energy Systems*, vol. 155, p. 109650, Jan. 2024, doi: 10.1016/J.IJEPES.2023.109650.

[9] L. Jia, S. Pannala, G. Kandaperumal, and A. Srivastava, “Coordinating Energy Resources in an Islanded Microgrid for Economic and Resilient Operation,” *IEEE Trans Ind Appl*, vol. 58, no. 3, pp. 3054–3063, 2022, doi: 10.1109/TIA.2022.3154337.

[10] B. Chen, J. Wang, X. Lu, C. Chen, and S. Zhao, “Networked Microgrids for Grid Resilience, Robustness, and Efficiency: A Review,” *IEEE Transactions on Smart Grid*, vol. 12, no. 1. Institute of Electrical and Electronics Engineers Inc., pp. 18–32, Jan. 01, 2021. doi: 10.1109/TSG.2020.3010570.

[11] F. Bandeiras, E. Pinheiro, M. Gomes, P. Coelho, and J. Fernandes, “Review of the cooperation and operation of microgrid clusters,” *Renewable and Sustainable Energy Reviews*, vol. 133. Elsevier Ltd, Nov. 01, 2020. doi: 10.1016/j.rser.2020.110311.

[12] S. Moussa and I. Slama-Belkhodja, “Residential loads modeling and load profile generation for microgrid EMS design in Tunisia,” *2022 IEEE International Conference on Electrical Sciences and Technologies in Maghreb, CISTEM 2022*, 2022, doi: 10.1109/CISTEM55808.2022.10043983.

[13] T. Sattarpour, S. Golshannavaz, D. Nazarpour, and P. Siano, “A multi-stage linearized interactive operation model of smart distribution grid with residential microgrids,” *International Journal of Electrical Power & Energy Systems*, vol. 108, pp. 456–471, Jun. 2019, doi: 10.1016/J.IJEPES.2019.01.023.

[14] A. Yazdani and I. Reza, *Voltage-Sourced Converters in Power Systems: Modeling, Control, and Applications | Wiley*. 2010. Accessed: Feb. 29, 2024. [Online]. Available: https://www.wiley.com/en-ca/Voltage+Sourced+Converters+in+Power+Systems+%3A+Modeling%2C+Control%2C+and+Applications-p-9780470521564

[15] M. A. Hasan and S. K. Parida, “An overview of solar photovoltaic panel modeling based on analytical and experimental viewpoint,” *Renewable and Sustainable Energy Reviews*, vol. 60, pp. 75–83, Jul. 2016, doi: 10.1016/J.RSER.2016.01.087.

[16] “Real-Time Simulation Communication Protocols | OPAL-RT,” 2022 - OPAL-RT TECHNOLOGIES, Inc. Accessed: Feb. 29, 2024. [Online]. Available: https://www.opal-rt.com/software-communication-protocols/

[17] “TCP/UDP - OPAL-RT - Communication Protocol,” 2022 - OPAL-RT TECHNOLOGIES, Inc. Accessed: Feb. 29, 2024. [Online]. Available: https://www.opal-rt.com/software-communication-protocols/tcp-udp/